One-pot facile synthesis of highly photoluminescent graphene quantum dots with oxygen-rich groups

Dai Yunqian   Sun Yibai   Long Huan   Chai Yunling   Sun Yueming

(School of Chemistry and Chemical Engineering, Southeast University, Nanjing 211189, China)

Abstract: To achieve a new type of carbon-based quantum dots with unique photoluminescence (PL), a simple approach for fabrication of graphene quantum dots (GQDs) with oxygen-rich groups was developed via the hydrothermal reaction by using graphene oxides (GOs) as a precursor. Transmission electron microscope (TEM) and atomic force microscope (AFM) characterizations confirmed that the sizes and heights of GQDs were (5. 02 ± 0. 92) nm and 0. 6 nm, respectively. A strong PL emission exhibited unique excitation wavelength dependent features. Also, the carbene-like free zigzag edge sites were proposed to be the origin of the strong PL emission. The GQDs were demonstrated to be a superior probe for Fe^{3+} detection in aqueous solution with a high sensitivity and feasibility, due to the special coordinate interaction between Fe^{3+} and the phenolic hydroxyl group at GQDs.

Key words: graphene; quantum dots; photoluminescence; oxygen-rich groups

doi: 10. 3969/j. issn. 1003 - 7985. 2014. 04. 020

The graphene sheet is a two-dimensional sheet consisting of sp^2-hybridized carbon atoms in a honeycomb lattice, and it has attracted tremendous research attention. The intrinsic thickness of the singe-layer graphene sheet is 0. 34 nm, and the lateral size of the graphene sheet can commonly range in the order of several hundred nanometers to tens of millimeters by using conventional chemical vapor deposition (CVD) and mechanical exfoliation etc. [1-5] In some recent work, "cutting" the lateral size of graphene down to 10 nm is an effective way of acquiring the unique optical characteristics, owing to the changes in electronic structures[5-6]. Also, the success of precise size controlling allows a new emergence of novel graphene derivation—the graphene quantum dots (GQDs) [7]. Their

quantum confinement and edge effect endow themselves with novel photoluminescence, which has been rarely observed in graphene[8]. To date, it is still of great challenge to facilely realize the GQDs directly from the pristine graphene sheet by the solution-phase-based approach, since the graphene sheet is usually insoluble in a solvent. Through many attempts, the GQDs have been synthesized via the electron-beam lithography, noble-metal-catalyzed C60 transformation, electrochemical or microwavable exfoliation of graphene derivation or carbon fibers etc[9-10]. Despite these recent developments, the above methods are limited to special equipment with a low yield. Also, the fabrication of GQDs is still far from a controllable manner, in particular regarding their functional groups at surfaces and/or edges sites.

One of the most popular graphene derivations is the graphene oxides (GOs), synthesized usually by exfoliation of oxidized natural graphite through a Hummers' method[11]. The GOs contains a high content of oxygen-rich groups, and thus are dispersible in many commonly used solvents. This vital feature ensures their success in acting as the precursor of GQDs. Also, the acquired GQDs most likely inherit the oxygen-rich groups from the pristine GOs, such as carboxyl, epoxide, hydroxyl groups.

In this regard, a new facile fabrication of GQDs was developed for this paper. The GQDs were hydrothermally cut from GOs into about 5 nm at 200℃ without any complex pre-treatment or special equipment. The GQDs had expectedly oxygen-rich functional groups and good qualities, with fewer defects and strong PL emission. The PL emission mechanism was also discussed. Moreover, their good water solubility and superior optical feature in aqueous solution allowed themselves to be fluorescent probes for Fe^{3+} detection due to their strong coordination interaction.

1 Experimental Section

1. 1 Hydrothermal fabrication of graphene quantum dots

Graphene oxides (GOs) colloids were prepared by a modified Hummer's method and acted as the starting carbon materials[12]. 1 g of graphite was ground with 0. 05 g NaCl and then washed with water to remove NaCl. 23

mL H_2SO_4(98%) was added and the solution was stirred for 22 h at room temperature. 6 g $KMnO_4$ was added slowly and the temperature was carefully kept below 20 ℃ using an ice bath. Afterwards, it was stirred at 40 ℃ for 30 min, then 90 ℃ for 45 min. The temperature was increased to 105 ℃ after adding 46 mL distilled water. 25 min later, the reaction was ended by adding 140 mL distilled water and 10 mL H_2O_2(30%) solution. The as-prepared graphite oxide product was washed with 5% HCl and then dialyzed with distilled water. 20 mg GOs colloids were first diluted with Millipore water and sodium hydroxide at a pH value of 8. Then the GOs colloids were carefully transferred into a Teflon-line stainless-steel autoclave, and a hydrothermal reaction was conducted at 200 ℃ for 10 h. After cooling down to room temperature, the GQDs were centrifuged at 15 000 r/min for 30 min then dried by a rotating evaporator. The purified GQDs were finally redispersed in Millipore water for dialyzing in a tubing bag (Molecular weight cut off is 3 500 Dalton) for one day.

1.2　Detection of Fe^{3+} in aqueous solution

The $FeCl_3$ was chosen as the Fe^{3+} source. 50 μL GQDs aqueous solution was first mixed with 50 μL Fe^{3+} solution. Then they were diluted by Millipore water, and their final volume was carefully controlled at a level of 500 μL. The PL spectra were monitored at an excitation wavelength of 320 nm and the PL peak intensities at 430 nm were recorded to calculate the quenching efficiency. The quenching efficiency was defined as $1 - I/I_0$, where I_0 is the pristine PL intensity of pure GQDs and I is the PL intensity with the varied concentration of Fe^{3+} solution.

1.3　Characterizations

The GQDs solution was dropped on an ultrathin carbon film supported on a copper grid with holes or silica wafer for observation under a transmission electron microscope (TEM) using a Tecnai G2 T20 (FEI); or for the measurement of Raman spectra tested by using a Thermo Fisher Scientific DXR Raman Microscope with a 532 nm laser beam. The Fourier transform infrared (FTIR) spectra were monitored by a Thermo Nicolet 5 700 spectrometer. The UV-vis spectra were recorded on a Shimadzu UV-2450 spectrophotometer and PL spectra were measured on a Horiba Jobin Yvon FluoroMax-4 spectrofluorometer. The height profiles of GQDs were tested by an atomic force microscope (AFM, Veeco). The quantum yields of the quantum dots were determined by using RhB as the standard sample, and were calculated according to the following equation:
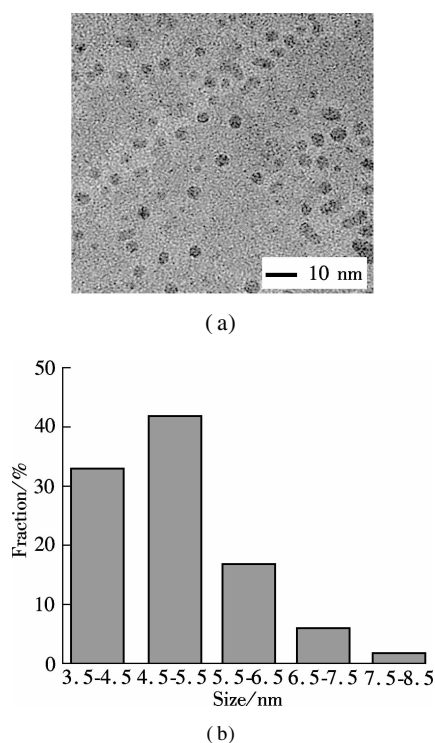
$$\Phi = \Phi_s(I'/I_s)(n^2/n_s^2)(A_s/A) \qquad (1)$$

where Φ is the quantum yield; I' is the measured integrated emission intensity; n is the refractive index; and A is the optical density. The subscript s refers to the standard sample (0.31 for RhB)[10].
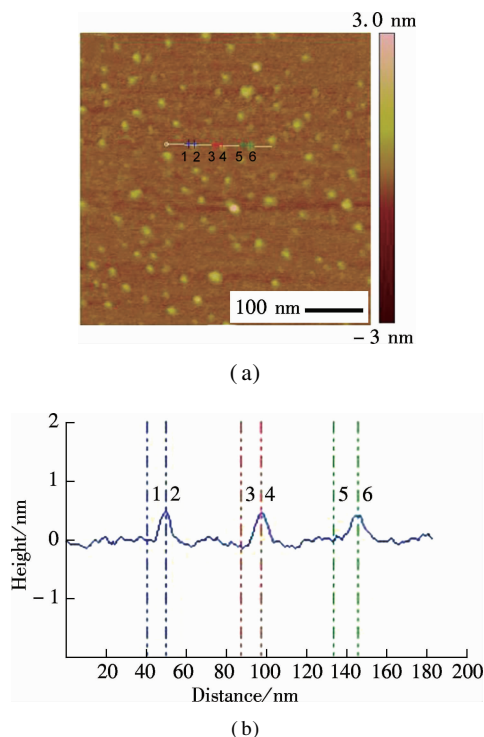
2　Results and Discussion

2.1　One-pot facile synthesis of the GQDs

The graphene quantum dots (GQDs) were hydrothermally fabricated in a NaOH solution (pH = 8) at 200 ℃ for 10 h, using GOs as the starting materials. As shown in Fig. 1(a), the GQDs had a tiny size less than 10 nm, and were evenly dispersed on the carbon grid with holes without any aggregation. A careful observation clarified that most GQDs had a circle periphery, although a few irregular shapes were also observed at a low frequency. The size distribution of GQDs is shown in Fig. 1(b), which have an average size of (5.02 ± 0.92) nm, by counting more than 100 GQDs.

(a)

(b)

Fig. 1　TEM characterizations of GQDs. (a) TEM image; (b) Size distribution diagram of GQDs fabricated in NaOH solution (pH = 8) at 200 ℃ for 10 h

To further illustrate the unique structure of GQDs, the atomic force microscope (AFM) is performed in a taping mode, which confirmed the uniform dispersion of GQDs without any aggregation (see Fig. 2(a)). The height profile indicates that the GQDs have a thickness of about 0.6 nm with a monolayer characteristic (see Fig. 2(b), labeled as 1 to 6)[13]. It is worth noting that the thickness of GQDs is slightly thicker than that of single-layer graphene with 0.34 nm, due to the presence of oxygen-rich functional groups. However, this thickness is consistent with that of the pristine GOs.
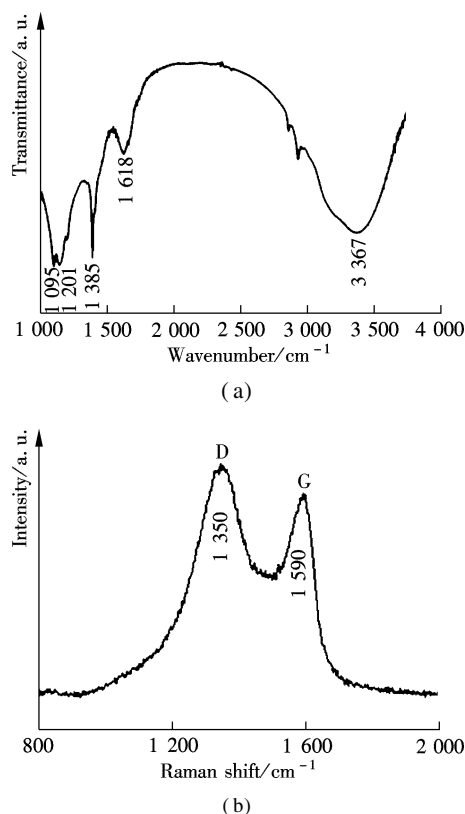
Fig. 2 AFM characterizations of GQDs. (a) AFM image of GQDs measured at a tapping mode; (b) Corresponding height profiles

2.2 Oxygen-riched groups and defects analysis

The presence of oxygen-rich functional groups in GQDs were evidenced in Fourier transform infrared (FTIR) spectra (see Fig. 3(a)). The GQDs showed a broad peak centered at 3 367 cm^{-1} and a sharp peak at 1 385 cm^{-1}, which were assigned to the stretching vibration of O—H groups. The vibration peaks of C—O at 1 095 cm^{-1} and C—OH at 1 201 cm^{-1}, further confirmed the adequacy of oxygen-rich groups. In addition, the sharp peak at 1 618 cm^{-1} belongs to the vibration of C—C in graphitic domains[14−15]. On the basis of the above results, the oxygen-rich groups in GQDs were well restored, most likely due to a high content of 52% oxygenate groups in the pristine GOs[12]. The oxygen-rich groups have been believed to be responsible for the good solubility and observed superior optical features in graphene oxide derivations[16], which allowed for their potential applications in imaging, sensing, drug delivery etc.

The Raman microscope is a powerful tool to analyze the intrinsic characters of carbon-based materials, such as defect and disorder. Fig. 3(b) shows two predominating bands in the Raman spectra of GQDs. The two bands are the D band at 1 350 cm^{-1} and the G band at 1 590 cm^{-1}[14−15]. The intensity ratio of the two bands I_D/I_G is an indicator of disorder, which is essential for their physicochemical properties, especially optical behavior. I_D/I_G of the GQDs was calculated to be 1.15, which was slightly higher than that of pristine GO (0.91)[12]. It is worth noting that, the sp^2 cluster sizes L_a is proportional
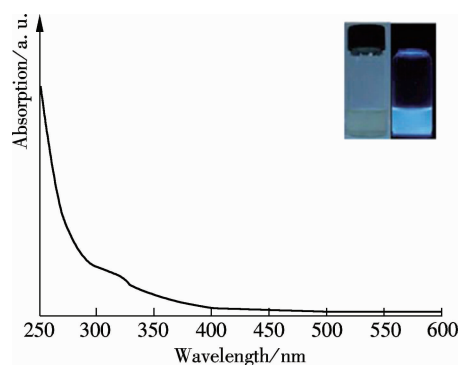

Fig. 3 Oxygen-riched groups and defects analysis. (a) FTIR; (b) Raman spectra of GQDs

to $(I_D/I_G)^{-1}$, while the distance between defects L_d is proportional to $(I_D/I_G)^{-1/2}$. Hence, "cutting" the sizes of GQDs down to about 5 nm led to a small cluster size and a short defect distance, most likely by generating disordered structures in a conjugated sp^2 cluster or at edge sites, therefore accelerating defect density[16]. However, I_D/I_G was still smaller than that of previously reported GQDs[17], indicating fewer defects and the good quality of GQDs by this one-pot facile reaction.
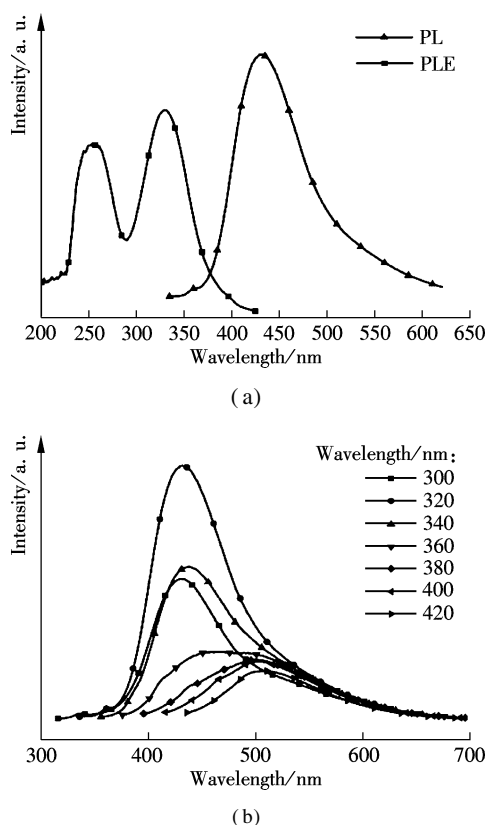
2.3 Optical properties of the GQDs

The UV-vis absorption spectrum of GQDs (see Fig. 4) shows a broadened absorption shoulder at 320 nm. This absorption was assigned to the π-π^* transition in the aromatic sp^2 domains[7]. The GQDs aqueous solution was in fact transparent and had a light yellow color, as shown in the inset of Fig. 4. Also, it did not exhibit any noticeable aggregation after storage for several months, indicating their good stability due to the presence of oxygen-rich functional groups. Interestingly, the GQDs emitted extensively blue photoluminescence under the irradiation of a 365 nm light, which was depicted in the inset in Fig. 4. The PL emission was highly stable and did not decay under the UV light illumination. The quantum yield of GQDs was tested to be 3.5%. The localized finite-sized sp^2 clusters was able to confine the electrons in the nanosized GQDs, and were proposed to be possibly responsible for their blue PL emissions[17].

Fig. 4 UV-vis spectrum of the GQDs. (The insets are the photographs of the GQDs under visible (left) and 365 nm UV light (right) irradiation.)
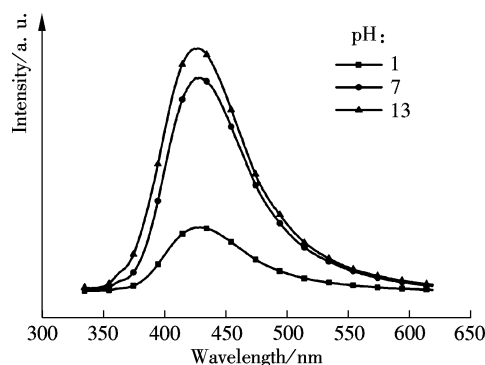
To uncover the unique optical properties of GQDs, the PL excitation (PLE) and PL spectra were performed, respectively. The PL excitation (PLE) spectra in Fig. 5 indicated that the recombination process of electron-hole pairs responded to the high photoluminescence emission. Interestingly, two distinct PLE peaks at 249 nm (4.98 eV) and 320 nm (3.88 eV) were observed, which indicated that two new types of electronically excited states contributed to the electron-hole recombination from the highest occupied molecular orbitals (HOMOs) to the lowest unoccupied molecular orbitals (LUMOs). An energy difference between the σ and π orbitals was 1.10 eV, which was within the required value (< 1.5 eV) for triple

(a)

(b)

Fig. 5 PLE and PL spectra of GQDs. (a) PLE (with the detection wavelength at 430 nm) and PL (under the excitation of 320 nm) spectra of GQDs; (b) PL spectra at different excitation wavelengths

carbenes by the Hoffman rule. Also, it conclusively implied that the two new types electron transitions from σ and π orbitals were the origin of strong emissions at emissive zigzag-edge sites[7]. As shown in Fig. 5(a), the GQDs emitted strong photoluminescence at 430 nm (2.88 eV), when excited at 320 nm (3.88 eV) with a Stökes shift of 110 nm (1.00 eV). Interestingly, the PL emission also exhibited excitation wavelength dependence (see Fig. 5(b)), that is, the emission wavelength accordingly red-shifted from 430 to 510 nm when the excitation wavelength red-shifted from 320 to 420 nm, and the PL intensity also gradually decreased.

To further understand the mechanism of PL emission, the PL spectra were tested when the pH of GQDs solution was adjusted to different values, as shown in Fig. 6. The GQDs emitted an approximately quenched PL emission in an HCl solution with pH = 1, while the enhanced PL emission in a NaOH solution with pH = 13, respectively. These observations were consistent with the feature of carbene-like emissive zigzag edge sites, which became inactive due to their protonation with H^+ and the breaking of carbene triple state under acid conditions[17]. While the carbene-like zigzag edge sites were well restored to be emissive after a reversible protonation process in alkaline conditions, this, therefore, led to the strong PL intensity. However, the PL peak position and shape remained the same. The pH-dependent PL emission inevitably confirmed the zigzag edge sites were the origin of the strong PL emission in the GQDs.
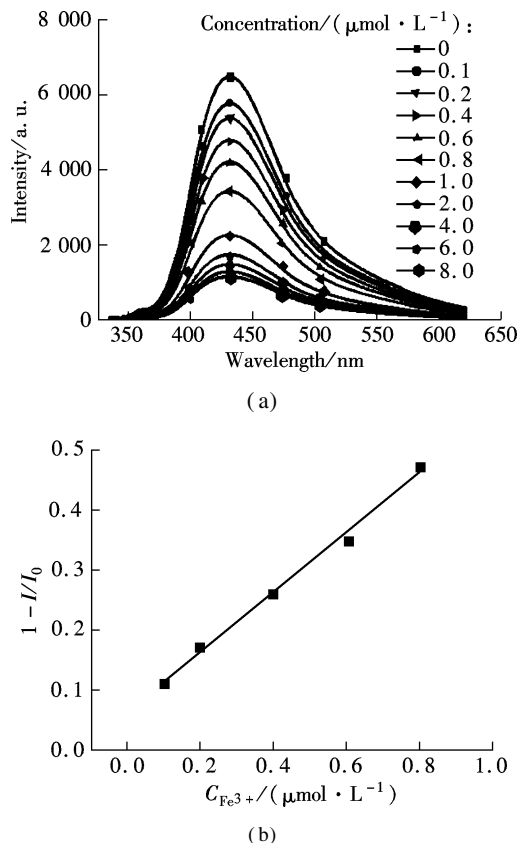

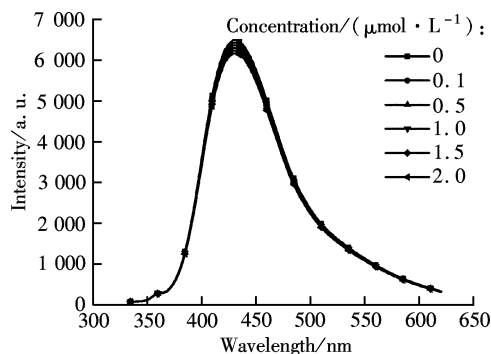**Fig. 6** PL spectra of the GQDs in water at different pH values when excited at 320 nm

2.4 The detection of Fe^{3+} in aqueous solution

With high water solubility, good optical stability, and strong PL emission ability, the GQDs were a newly emerging good candidate to be an efficient fluorescent probe in aqueous solution. However, many important cations in human body, including Fe^{2+}, Na^+, K^+, Mg^{2+}, Ca^{2+}, Zn^{2+}, Co^{2+}, Cu^{2+}, cannot efficiently quench their PL emission by the π-π stacking mechanism[18]. The ferric (Fe^{3+}) ions play a vital role in a human body, since they anticipate many important biological processes, including

red cells reproduction, oxygen transportation, and DNA copying. The concentration of Fe^{3+} in a human body is low and commonly ranges from μmol/L to mmol/L, but the imbalance of Fe^{3+} ions usually leads to many diseases[19]. Therefore, the detection of Fe^{3+} by a quick and facile approach is of great urgency. The photoluminescence strategy is one of the most promising methods for quantitatively detecting Fe^{3+} ions in aqueous solution, due to its high sensitivity and feasibility. Interestingly, the PL intensity of GQDs gradually decreases with the increase in Fe^{3+} concentration (see Fig. 7(a)). Also, the PL emission is quenched quickly in only 1 min, and no further decrease of PL intensity can be detected in a longer reaction time, indicating that the quenching reaction reaches equilibrium in a rapid fashion. Around 9% of the PL emission is quenched at 0. 1 μmol/L Fe^{3+} ions, and it is mostly completely quenched in 8. 0 μmol/L Fe^{3+}. Therefore, the GQDs have a wide detection range from 0 to 8. 0 μmol/L. The quenching efficiency of GQDs shows a linear relationship with the Fe^{3+} concentration, ranging from 0 to 0. 8 μmol/L ($R = 0. 998$) (see Fig. 7 (b)). Furthermore, no observable PL peak shift occurs, and the PL shape is well retained after the occurrence of PL quenching.

(a)

(b)

Fig. 7 The detection of Fe^{3+} in aqueous solution. (a) The PL spectra of GQDs in the presence of Fe^{3+} with the concentration varying from 0 to 8. 0 μmol/L; (b) The linear relationship between C_{Fe3+} and the quenching efficiency

Fig. 8 The PL spectra of GQDs in the presence of NaCl with varied concentrations

Next, to investigate the quenching mechanism, we conduct some control experiments in the presence of NaCl, as shown in Fig. 8. In contrast, the presence of NaCl salt does not cause the undesirable quenching of PL emission or PL peak shift, even when its concentration reaches 2. 0 mol/L. The result evidently indicates the negligible role of Cl^- anions and Na^+ cations in quenching PL emission, and the desirable selectivity of GQDs towards to Fe^{3+}. It is known that the GQDs are negative charged in water[20]. Therefore, the cations easily absorb on their surface and/or edges by electrostatic interaction. However, this weak interaction is not able to induce PL quenching, since the presence of Na^+ does not decrease the PL emission. In fact, Fe^{3+} has a half-filled $3d^5$ orbitals on the outer electronic structure, and easily accepts electrons from donors, such as those on the conductive band and/or defect-related band of GQDs[20], by the coordinate interaction between Fe^{3+} and phenolic hydroxyl group at GQDs. As a result, the efficient electron transfer led to depressed radiative recombination of electron-hole pairs, and, thus, the observed PL quenching. This special coordinate interaction between Fe^{3+} and the GQDs surfaces also ensures their good selectivity in aqueous solution. That is, many important cations, such as Ni^{2+}, Ag^+, Cd^{2+}, Hg^{2+}, cannot efficiently quench the PL emission of GQDs, in addition to above mentioned cations[19]. Taken together, the GQDs exhibited a rapid response and high sensitivity to Fe^{3+} ions, and can act as a new type of fluorescent probe for the Fe^{3+} detection in aqueous solution.

3 Conclusion

In this paper, the highly photoluminescent GQDs were prepared by a one-pot facile hydrothermal reaction in a NaOH solution. This method is simple, low-cost, time-saving, and reliable without using any complex equipment. The GQDs have an average size of about 5 nm and a uniform thickness of 0. 6 nm. The FTIR and Raman spectra reveal the presence of large amounts of oxygen-rich functional groups, fewer defects and good qualities. They exhibit strong PL emission arising from the emissive

zigzag-edge sites. The GQDs are further confirmed as the efficient fluorescent probe for Fe^{3+} detection in water, and exhibit a rapid response, are highly sensitive and have good selectivity as the result of strong electron transfer from the GQDs to the half-filled $3d^5$ orbitals at Fe^{3+}. This paper inspires an efficient approach for engineering the superiorly intrinsic features of graphene derivation, particularly photoluminescence.

References

[1] Novoselov K S, Geim A K, Morozov S V, et al. Electric field effect in atomically thin carbon films [J]. *Science*, 2004, **306**(5696): 666 − 669.

[2] Meyer J C, Geim A K, Katsnelson M I, et al. The structure of suspended graphene sheets [J]. *Nature*, 2007, **446**(7131): 60 − 63.

[3] Yazyev O V, Louie S G. Electronic transport in polycrystalline graphene [J]. *Nature Materials*, 2010, **9**: 806 − 809.

[4] Wei Z, Wang D, Kim S, et al. Nanoscale tunable reduction of graphene oxide for graphene electronics [J]. *Science*, 2010, **328**(5984): 1373 − 1376.

[5] Jiao L, Wang X, Diankov G, et al. Facile synthesis of high-quality graphene nanoribbons [J]. *Nat Nanotechnol*, 2010, **5**: 132 − 132.

[6] Xie L, Wang H, Jin C, et al. Graphene nanoribbons from unzipped carbon nanotubes: atomic structures, Raman spectroscopy, and electrical properties [J]. *J Am Chem Soc*, 2011, **133**(27): 10394 − 10397.

[7] Gupta V, Chaudhary N, Srivastava R, et al. Luminscent graphene quantum dots for organic photovoltaic devices [J]. *J Am Chem Soc*, 2011, **133**(26): 9960 − 9963.

[8] Gokus T, Nair R, Bonetti A, et al. Making graphene luminescent by oxygen plasma treatment [J]. *ACS Nano*, 2009, **3**(12): 3963 − 3968.

[9] Lu J, Yeo P S E, Gan C K, et al. Transforming C60 molecules into graphene quantum dots [J]. *Nature Nanotechnology*, 2011, **6**(4): 247 − 252.

[10] Peng J, Gao W, Gupta B, et al. Graphene quantum dots derived from carbon fibers [J]. *Nano Lett*, 2011, **12**(2): 844 − 849.

[11] Hummers W S Jr, Offeman R E. Preparation of graphitic oxide [J]. *J Am Chem Soc*, 1958, **80**(6): 1339.

[12] Dai Y, Jing Y, Zeng J, et al. Nanocables composed of anatase nanofibers wrapped in UV-light reduced graphene oxide and their enhancement of photoinduced electron transfer in photoanodes [J]. *J Mater Chem*, 2011, **21**(45): 18174 − 18179.

[13] Morales-Narváez E, Merkoçi A. Graphene oxide as an optical biosensing platform [J]. *Adv Mater*, 2012, **24**(25): 3298 − 3308.

[14] Shen J, Shi M, Yan B, et al. One-pot hydrothermal synthesis of Ag-reduced graphene oxide composite with ionic liquid [J]. *J Mater Chem*, 2011, **21**: 7795 − 7801.

[15] Zhu C, Guo S, Wang P, et al. One-pot, water-phase approach to high-quality graphene/TiO₂ composite nanosheets [J]. *Chem Comm*, 2010, **46**(38): 7148 − 7150.

[16] Li Y, Zhao Y, Cheng H, et al. Nitrogen-doped graphene quantum dots with oxygen-rich functional groups [J]. *J Am Chem Soc*, 2011, **134**(1): 15 − 18.

[17] Pan D, Zhang J, Li Z, et al. Hydrothermal route for cutting graphene sheets into blue-luminescent graphene quantum dots [J]. *Adv Mater*, 2010, **22**(6): 734 − 738.

[18] Li L, Wu G, Hong T, et al. Graphene quantum dots as fluorescence probes for turn-off sensing of melamine in the presence of Hg^{2+} [J]. *ACS Appl Mater Interfaces*, 2014, **6**(4): 2858 − 2864.

[19] Zhou L, Geng J, Liu B, et al. Graphene quantum dots from polycyclic aromatic hydrocarbon for bioimaging and sensing of Fe^{3+} and hydrogen peroxide [J]. *Particle & Particle Systems Characterization*, 2013, **30**(12): 1086 − 1092.

[20] Mei Q, Jiang C, Guan G, et al. Fluorescent graphene oxide logic gates for discrimination of iron ($^{3+}$) and iron ($^{2+}$) in living cells by imaging [J]. *Chemical Communications*, 2012, **48**(60): 7468 − 7470.

一步法合成富氧基团石墨烯量子点及光致发光特性

代云茜　孙贻白　龙　欢　柴蕴玲　孙岳明

(东南大学化学化工学院,南京 211189)

摘要:为获得独特的光致发光特性的碳基量子点,以氧化石墨烯(GOs)为前驱物,采用水热反应合成了一类富氧官能团修饰的石墨烯量子点(GQDs). TEM 和 AFM 表征 GQDs 平均粒径为(5.02 ±0.92) nm,厚度为 0.6 nm. GQDs 呈现特有的光致发光峰位随激发波长移动的特性,其光致发光机理来源于量子点边缘的类卡宾 zigzag 活性位. 由于 Fe^{3+} 与 GQDs 表面羟基的配位作用使 GQDs 呈现出对 Fe^{3+} 离子检测的高灵敏度和快速响应,有望成为高效检测 Fe^{3+} 离子的新型荧光探针.

关键词:石墨烯;量子点;光致发光;富氧官能团

中图分类号:O613.7